ORIGINAL PAPER - PARTICLES AND NUCLEI

Design and fabrication of side-coupled RF cavity for S-band 6/3 MeV dual-energy electron linac

Jungho Mun[1] · Moonsik Chae[1] · Jaehyun Lee[1] · Yeong Henm Yeon[1] · Jae Yeon Park[1] · Nam Ho Lee[1]

Abstract

We demonstrate the design and manufacture of RF (radio-frequency) electron linac (linear accelerator) cavity of 6/3 MeV dual-energy X-ray generator for air-cargo security inspections. When an accelerated electron beam collides with the metal target, an X-ray is generated by a bremsstrahlung process. We designed a dual-energy RF cavity using a three-dimensional electromagnetic field simulation code and an electron beam trajectory code. The designed RF cavity is a side-coupled standing-wave type, driven by the $\pi/2$ mode, and has a resonant frequency of 2856 MHz. The maximum dose rate of X-ray was calculated to be 7.07 and 0.91 Gy/min at 1 m for an X-ray energy of 6 and 3 MeV using a tungsten target, respectively. In the simulation results, the accelerating gradient was about 13.5 MV/m, the Q-factor was 15,900, and the total length of the RF cavity was 57 cm for 6 MeV of the maximum accelerated electron energy. The resonance frequency and the Q-factor of the fabricated RF cavity were measured by 2855.34 MHz and 14,000, respectively.

Keywords RF cavity · X-ray · S-band · Side-coupled cavity · Security inspection

1 Introduction

X-ray generators that use electron accelerators are being used as useful tools in various research fields such as medical, security inspection, nondestructive testing, nuclear engineering, and semiconductor materials. The required energy for the electron beam, the beam output power, and the operation method are different depending on the applications. In particular, the low-energy electron accelerators that range from a few hundred keV to a few MeV are relatively simple in structure and can be manufactured in a small size of several meters, which have great commercial advantages in terms of miniaturization and cost reduction [1, 2]. In recent years, the demand for low-energy electron accelerator-based X-ray generators has been increasing due to the security inspection for containers that are rapidly increasing at both airports and sea ports. Since the X-ray has a good penetration ability, it is possible to search for weapons and smuggled goods in the container without opening them. In the dual-energy X-ray generators, the different attenuation

of X-ray pulses can achieve the transmission image and material discrimination [2–9]. Recently, the Korea Atomic Energy Research Institute (KAERI) has developed an electron accelerator-based 9/6 MeV dual-energy X-ray generator for port container security inspection systems [10]. The dual-energy X-ray generator can distinguish the organic/inorganic information of an object, but there is a limit in being able to precisely distinguish substances such as explosives, which are made of elements such as carbon, oxygen, and nitrogen. Using a security inspection system that combines X-rays with neutrons can improve the capability of discriminating materials. Therefore, an inspection system that uses the dual-energy X-rays and neutrons simultaneously can distinguish the shape and material of the object, as well as distinguish the nuclear and explosive materials [11].

In this paper, we will demonstrate the design and fabrication of a RF electron accelerator for a 6/3 MeV dual-energy X-ray generator for air-cargo inspections. The RF cavity is a core device of an electron accelerator that accelerates electrons to high energy using a strong electric field formed in the RF cavity. Generally, the structure of the RF cavity can either be an on-axis π-mode type, an on-axis $\pi/2$ mode, and a bi-periodic side-coupled $\pi/2$ mode type. The on-axis π-mode type can be manufactured with a relatively simple structure, and the manufacturing and maintenance costs are

✉ Jungho Mun
jhmun@kaeri.re.kr

1 Radiation Research Division, Korea Atomic Energy Research Institute, Jeongeup 56212, South Korea

lower than the other structures, but its shunt impedance is low. In addition, the narrow mode separation in the on-axis π-mode type can cause the electron beam to have an unstable output power. The $\pi/2$ mode RF cavity has a higher shunt impedance than the π-mode RF cavity. It also has the advantage of operating at a wide mode separation. In particular, in the case of a small-size electron accelerator that uses an RF source with a limited output power, a bi-periodic side-coupled $\pi/2$ mode type that has a high shunt impedance and is small in size has good acceleration efficiency [11–14]. In this study, the designed RF cavity was a side-coupled standing-wave type, driven by a $\pi/2$ mode, and the resonant frequency was 2856 MHz (S-band).

2 Accelerating RF cavity design

1. Design features of an RF cavity

An accelerated electron beam current can be obtained by calculating the dose rate of the bremsstrahlung X-ray generated by the accelerated electron beam colliding against the metal target. The dose rate of the X-ray is calculated as follows [11–16]:

$$J_x = c \cdot \eta \cdot D \cdot I_b \cdot E^n, \tag{1}$$

where c is the capture coefficient, which represents the rate at which the electron beam generated from the electron gun enters the RF cavity, D is the duty factor multiplied by the pulse width and the repetition rate of an input RF pulse, I_b is the peak current of the accelerated electron beam, E is the energy of the accelerated electron beam, and n is the energy factor of the accelerating electron beam. η is the electron–photon conversion efficiency when the electron beam collides with a specific metal target. Table 1 shows the calculation results of the dose rate of 6/3 MeV dual-energy X-rays using the X-ray generation target as tungsten. If the peak current of the electron beam is 200 mA at the capture coefficient of 0.5, then the X-ray dose rates for the accelerated electron beam energy 6 and 3 MeV should be calculated as 7.07 and 0.91 Gy/min at 1 m, respectively. The

required dose rate was referred to Refs. [7–9] for a cargo security inspection. In addition, it is possible to increase the dose rates by increasing the repetition rate and pulse width of input RF pulse.

The acceleration voltage of the electron beam in the standing-wave linear accelerator is expressed as [17, 18]

$$V = \frac{2\sqrt{\beta_0}}{1 + \beta_0}\sqrt{P_{RF}rl}\cos\varphi - \frac{rl}{1 + \beta_0}I_b, \tag{2}$$

where β_0 is the coupling coefficient of the power coupler, P_{RF} is the RF power input to the accelerating cavity, r is the effective shunt impedance, l is the total length of the accelerating cavity, and I_b is the peak current of the accelerated electron beam. Table 2 shows the main design parameters of the RF cavity for calculating the acceleration voltage. The total length of the accelerating cavity is approximately 0.6 m considering the acceleration gradient (10 MV/m) of the RF cavity for a compact accelerator with a maximum acceleration voltage of 6 MV. The effective shunt impedance of the accelerating cavity calculated by the SUPERFISH code is about 100 MΩ/m. The entire RF cavity consists of bunching and accelerating sections. The bunching section has a lower shunt impedance than the accelerating section, and the total shunt impedance of the entire RF cavity is approximately 90 MΩ/m with a 10% reduction rate. The power coupling coefficient is 2.8, considering the beam loading effect. The power coupling coefficient was calculated by the following equation [18]:

$$\beta_0 = 1 + \frac{P_b}{P_c}, \tag{3}$$

where P_c is the power dissipation in the cavity wall, and P_b is the loading beam power. We found that $P_c = 0.667$ MW and $P_b = 1.2$ MW at $I_b = 200$ mA. Then we obtain $\beta_0 = 2.799$.

Figure 1 shows the calculation results of the accelerated electron beam energy as a function of the input RF power at the peak current of the 200 mA electron beam. The required input RF power for the 6/3 MeV energy of the accelerating electron beam is about 1.87/0.82 MW, respectively.

Table 3 shows the design goal of the 6/3 MeV dual-energy electron accelerator cavity. The effective shunt impedance is more than 90 MΩ/m, and the acceleration gradient of the RF cavity is about 10 MV/m in consideration of the maximum

Table 1 The calculation parameters and results of dose rate (J_x) of 6/3 MeV dual-energy X-rays

Parameter	description	6 MeV	3 MeV
c	Capture coefficient	0.5	0.5
η	Photon conversion efficiency	0.0669	0.0271
I_b (mA)	Beam peak current	200	200
D	Duty factor	0.0007	0.001
N	Electron energy factor	2.8	3.2
J_x (Gy/min @ 1 m)	X-ray dose rate	7.07	0.91

Table 2 The main design parameters of the RF cavity for calculating the acceleration voltage

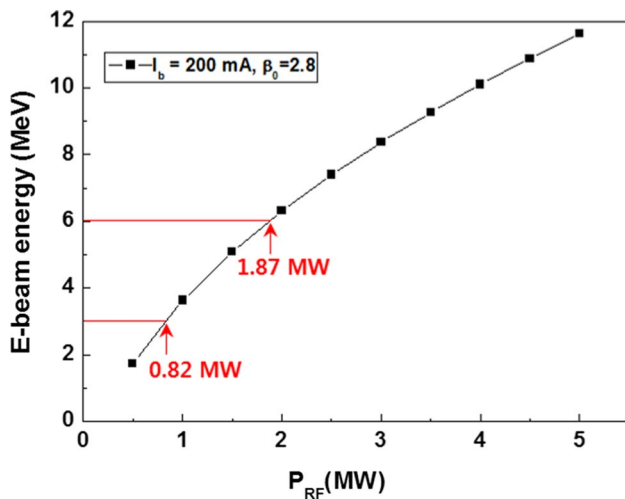|	
l, length of cavity (m)	0.6
r, effective shunt impedance (MΩ/m)	90
β_0, coupling coefficient	2.8
I_b, beam peak current (A)	0.2
V, accelerated beam energy (MeV)	3, 6

Fig. 1 The acceleration energy of the electron beam as a function of the input RF power (P_{RF}) at the peak current of the 200 mA electron beam

Table 3 The design goals of the 6/3 MeV dual-energy electron accelerator cavity

Design goals (S-band, $\pi/2$ mode)	
Frequency (MHz)	2856
Q-factor (unloaded)	> 12,000
Effective shunt impedance (MΩ/m)	~ 90
Coupling coefficient	~ 2.8
E-field gradient (MV/m)	~ 10
Total length of cavity (m)	~ 0.6

electron beam current and the required input RF power in the X-ray dose rate calculation. The total length of the acceleration cavity is about 60 cm for accelerating the maximum energy of a 6 MeV-electron beam.

2. **2**-D and 3-D simulation of single cells

In a compact electron accelerator with a limited RF power, it is very important to increase the acceleration efficiency of the RF cavity to accelerate the electron beam of the MeV class, even in a short-length cavity. Two-dimensional (2-D) simulation of the accelerating cavity cells was performed using a SUPERFISH code. To maximize the acceleration efficiency of the RF cavity, the effective shunt impedance (ZT^2) was maximized and the breakdown voltage (E_m/E_0) was minimized in this design. Figure 2 shows the acceleration cavity structure (half of the symmetric acceleration cell) designed using the SUPERFISH code. Figure 2a shows the simulation results of the bunching cell. The z-axis length of the bunching cell was set to 26.24 mm, which corresponds to a β ($= v/c$, v is the electron beam velocity, and c is the light velocity) value of 0.5. As a result of simulation, $ZT^2 = 71.86$ MΩ/m and $E_m/E_0 = 3.0973$. In the simulation results of the acceleration cell, as shown in Fig. 2b, the length of the acceleration cell is 52.48 mm, which corresponds to $\beta = 1$, $ZT^2 = 104.85$ MΩ/m, and $E_m/E_0 = 3.8193$.

Three-dimensional (3-D) simulation of single cells from the RF cavity was performed using a 3-D electromagnetic analysis code based on the geometrical structure of the cavity cell, which is the result of the SUPERFISH code. As in the 2-D computer simulation, the RF electron accelerator cavity is designed to have a maximum Q-factor and a maximum ZT^2 to realize a structure that has the maximum acceleration efficiency in a short cavity length. Finally, we can get the solution of fundamental modes, such as field distribution, resonant frequencies, and so on. Figure 3 shows the designed structure of single cells from an electron accelerator using a 3-D electromagnetic analysis code. The arrow is also the electric field direction in the acceleration cavity.
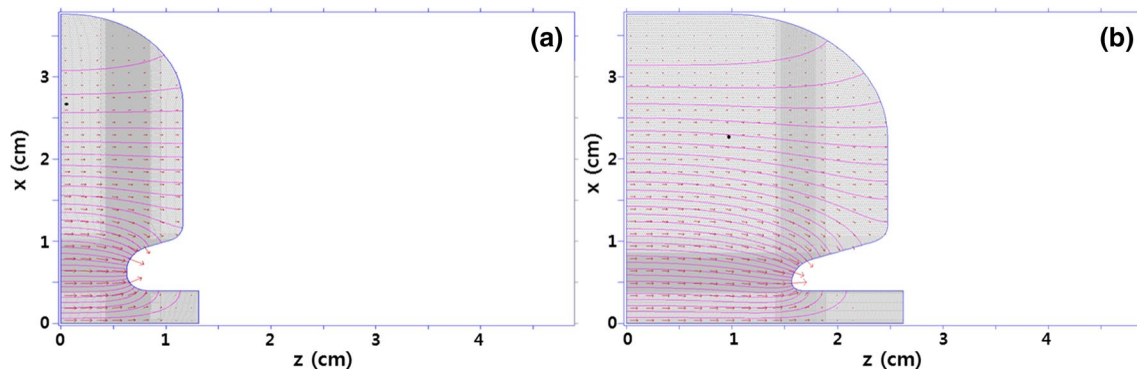

Fig. 2 The acceleration cavity structure (half of the symmetric acceleration cell) designed using the 2-D SUPERFISH code
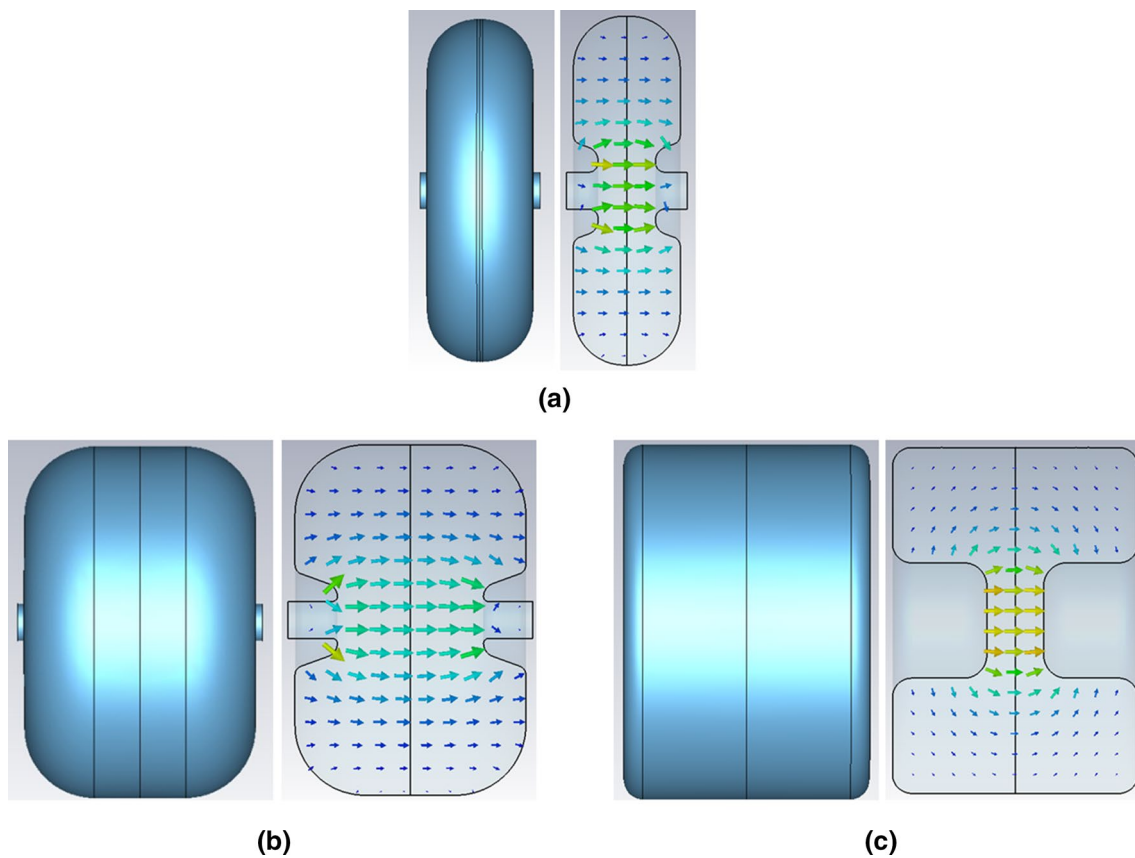
Fig. 3 The 3-D simulation results of single cells, and the arrow is the electric field direction in the single cells. **a** Bunching cavity cell, **b** acceleration cavity cell, **c** side-coupling cavity cell

Figure 3a shows the simulation results of the bunching cavity cell (BC). The BC is designed to maximize the acceleration efficiency of the electron beam, that is, the Q value and the effective shunt impedance. The direction of the arrow in Fig. 3 represents the direction of the electric field on the cavity axis (z-axis). As indicated in the simulation results, the resonance mode is the TM_{010} in BC, and the resonant frequency is 2887.4 MHz, which is higher than the expected 2856 MHz, considering the coupling between the side-coupling cavity cells (SC) and the accelerating cavity cell (AC). The length of BC is 26.24 mm and $\beta = 0.5$. As a result, the effective shunt impedance is 70.87 MΩ/m, and the Q value is 11946. An eigenmode simulation of a single AC and SC with a maximum Q and ZT^2 was performed. Figure 3b shows the structure and electric field distribution of AC as a result. The resonance mode is TM_{010}, and the resonant frequency is 2882.02 MHz, considering the coupling between SC and AC. The length of AC is 52.48 mm ($\beta = 1$), and the effective shunt impedance and Q value are a maximum of 103.5 MΩ/m and 16,984.6, respectively. The SC in Fig. 3c is a cylinder type structure and serves as a coupler that allows the RF field to be transported well by AC to accelerate the electron beam. The electric field of SC is

zero in the $\pi/2$ mode structure. As a result of the eigenmode simulation of the single SC, the resonance frequency and Q value are 2934.57 MHz and 8070.3, respectively.

To optimize the entire side-coupled cavity, inter-cell coupling simulation was performed with the single-cavity-cell chain, which is a combined structure of AC and SC. As shown in Fig. 4, the side-coupled cavity has two basic single-cavity-cell chain structures, which are the different structures of AC and SC combinations.

Figure 4a, b shows the ASA and SAS cell chains. The ASA cell chain forms two half ACs (hAC) on both sides of the SC. The SAS cell chain forms two half SCs (hSC) on both sides of the AC. The frequency difference of the two cell chains on the $\pi/2$ mode is called the stop band. To make sure the entire RF cavity operates in a $\pi/2$ mode, the geometrical structures of the ASA and SAS cell chains must be adjusted to make the stop band as small as possible.

Figure 4a, b shows the electric field distribution in three basic modes, which is the simulation result of the ASA and SAS cell chains and its structure. When the electric field direction changes $\pm z$, 0, and $\mp z$ for each cell, the phase change between each cell is 90°. At this time, the electric field resonates in the $\pi/2$ mode, electrons can be accelerated
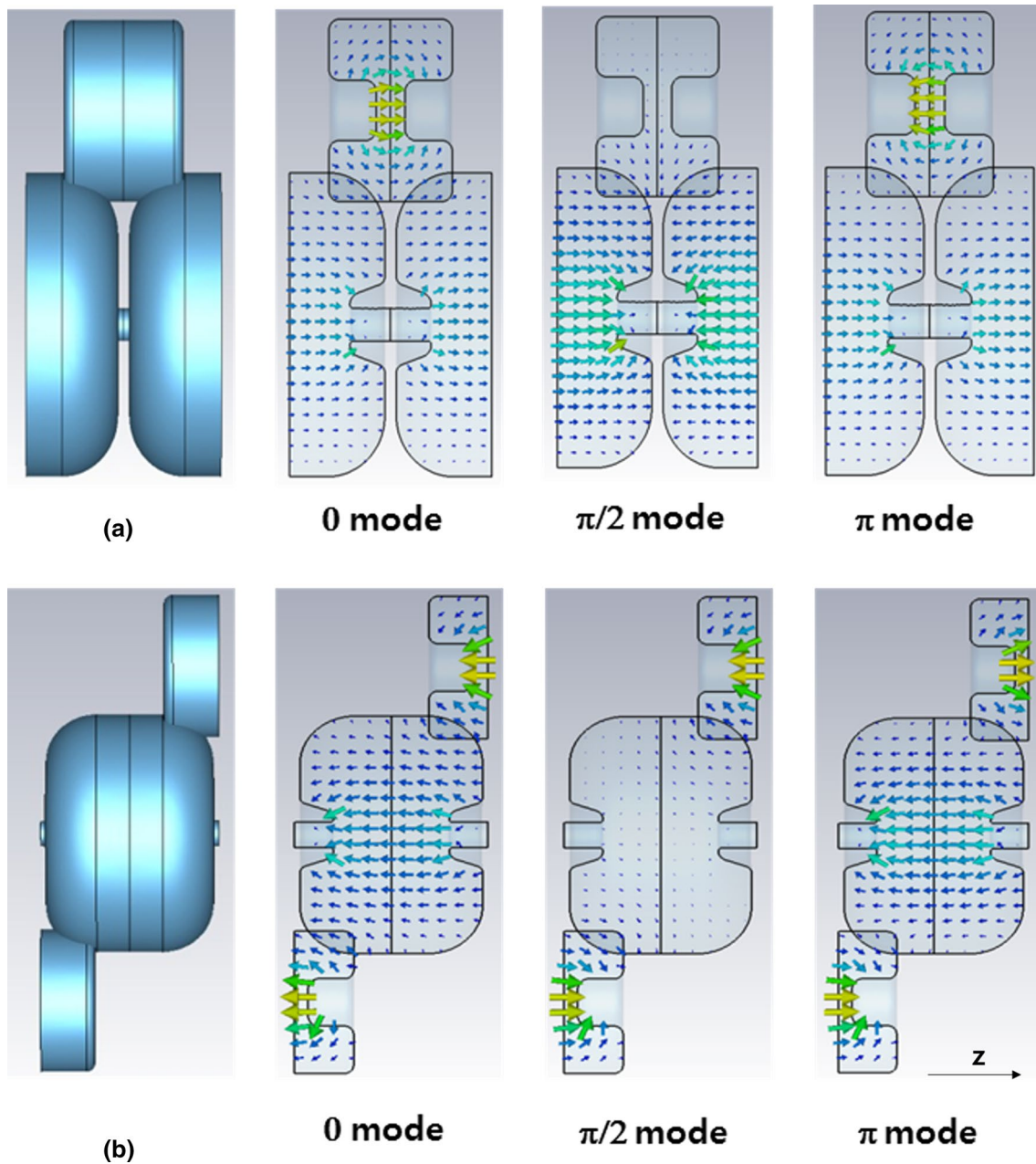
Fig. 4 The structures of single-cell-cavity chains and the electric field distribution in three basic modes. **a** ASA cell chain, **b** SAS cell chain

while passing through the RF cavity. The resonance frequencies were calculated 2856.2 and 2855.85 MHz in each single-cavity-cell chain (ASA and SAS) when the coupling coefficient is 3.5% $\left(k = \frac{f_\pi - f_0}{f_{\frac{\pi}{2}}} = 0.035 \right)$. The stop band between the two single-cavity-cell chains is 0.35 MHz. Through the minimization of the stop band between the cell chains, a target resonant frequency of 2856 MHz is realized in the combined single-cavity cell chain structure with AC and SC having different resonance frequencies [19, 20].

The generated RF power from the RF source such as magnetron or klystron is fed into the RF cavity through the power coupler. Figure 5 shows the schematics of the entire cavity cell with the power coupler. The power coupler consists of a rectangular waveguide, tapered waveguide, and power coupling cavity cell (PC). The PC has a coupling slot on the top wall of the cell and is directly connected to the tapered waveguide, and the RF power is fed to the RF cavity through the waveguide port (red part), which is located on the top plane of the rectangular waveguide, as shown in Fig. 5. With an operating frequency of 2856 MHz, the type
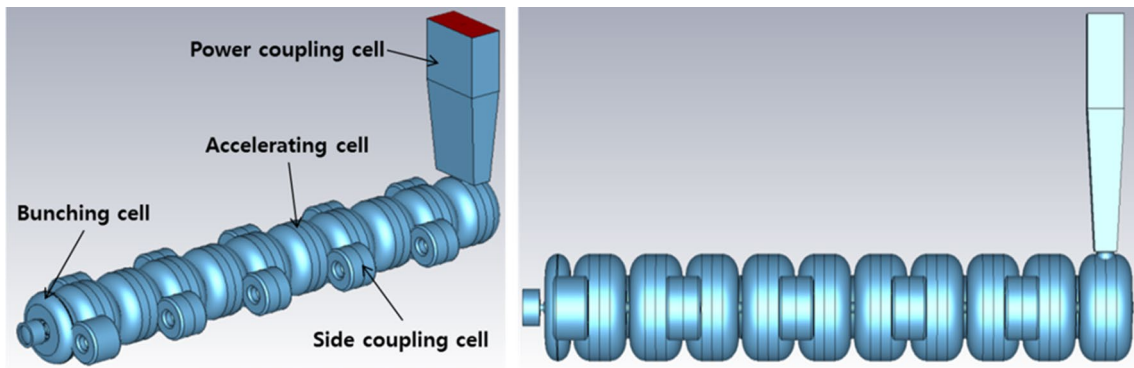
Fig. 5 The schematics of the entire cavity cell with power coupler

of R-32 rectangular waveguide was selected. The entire RF cavity consists of 1 BC, 10 SC, and 10 AC, which are a total of 21 cells.

3. Simulation of whole cell cavity

Figure 6 shows the eigenmode simulation results of the entire dual-energy electron cavity, including the power coupling cell.

In Fig. 6a, the electric field distribution of the designed cavity is $\pi/2$ mode, and the simulation results of the resonance frequency are 2855.7 MHz, the Q_0 is 15976, and the Q_{ext} is 5622. The coupling coefficient between the power coupling cell and the entire acceleration cavity cell is $\beta_c = Q_0/Q_{ext} \sim 2.8$. In addition, we found that the effective shunt impedance is 87 MΩ/m, and the acceleration gradient of the total accelerating cavity satisfies the design value of about 13.5 MV/m when the stored energy of the accelerating cavity is 1 J. For the stable operation of the designed RF cavity, the mode separation between the resonant frequency of the operating mode and the neighbor mode frequency has to be sufficiently wide. The mode separation of the RF cavity

Fig. 6 The eigenmode simulation results of the entire dual-energy electron cavity, including the power coupling cell. **a** The electric field distribution in the cavity cell, **b** the electric field profile along the z-axis
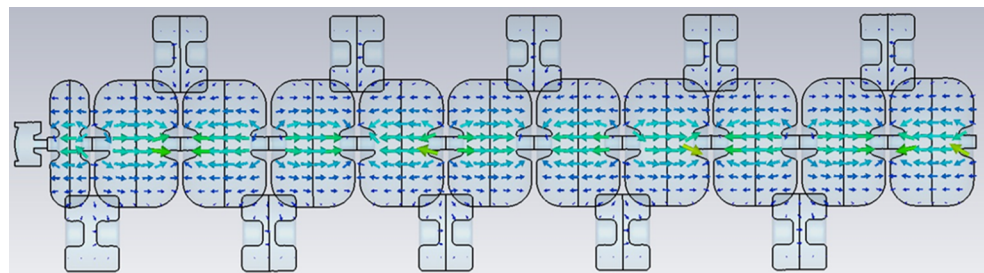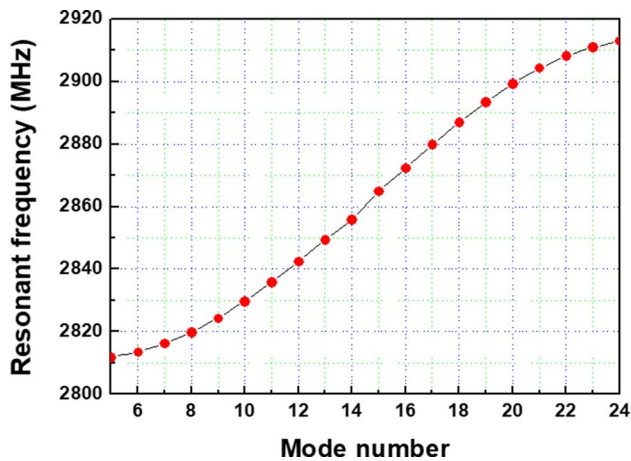

(a)
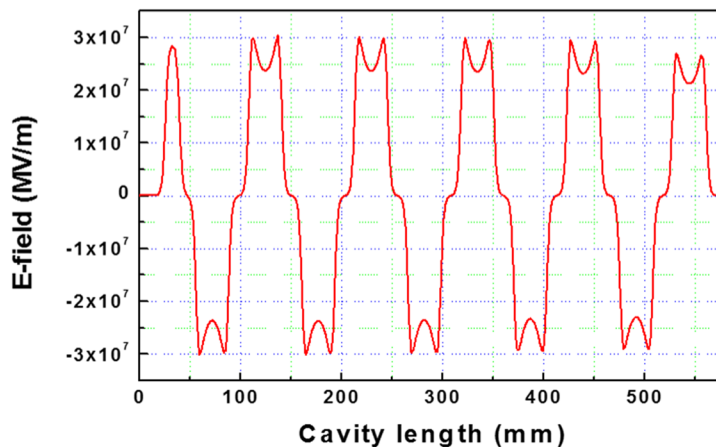
(b)

Fig. 7 Dispersion curve for a designed cavity

in this study can be confirmed by the dispersion curve of the total acceleration cell in Fig. 7.

The operating mode ($\pi/2$ mode) is the 14th mode in Fig. 7. The mode separation between the $\pi/2$ mode and the nearest modes (13th and 15th) is ± 8 MHz. Considering the frequency ranges of the magnetron are ± 5 MHz, the designed cavity has stable operating conditions.

The coupling coefficient (β_c) calculated using the Q value as a result of the eigenmode simulation of the entire acceleration cell was 2.8. Since the coupling coefficient is a very important parameter in designing the electron accelerator, the scattering-parameter (S-parameter) simulation of the entire acceleration cell was performed. The S-parameter is the ratio of the output to input RF power in dB. In addition, the coupling coefficient between the power coupler and the accelerating cavity can be determined by measuring the reflection signal of the RF frequency. Figure 8 shows the S-parameter simulation results of the designed dual-energy electron accelerator cavity. The voltage standing-wave ratio (VSWR) was calculated using the S-parameter simulation results, and we found the coupling coefficient was 2.68 from VSWR. The coupling coefficient of the RF cavity designed through the eigenmode and S-parameter simulation satisfied the design value of 2.8. Table 4 shows the final simulation results of the dual-energy electron accelerator cavity:

4. Beam dynamics simulation

Based on the simulation results of the designed RF cavity using the 3-D electromagnetic field analysis code, the electron beam dynamics were analyzed using the ASTRA code. This is to confirm whether the electron beam accelerated to the target energy in the designed RF cavity. Figure 9 shows the simulation results of the accelerated electron beam energy at an X-ray target position 80 cm away
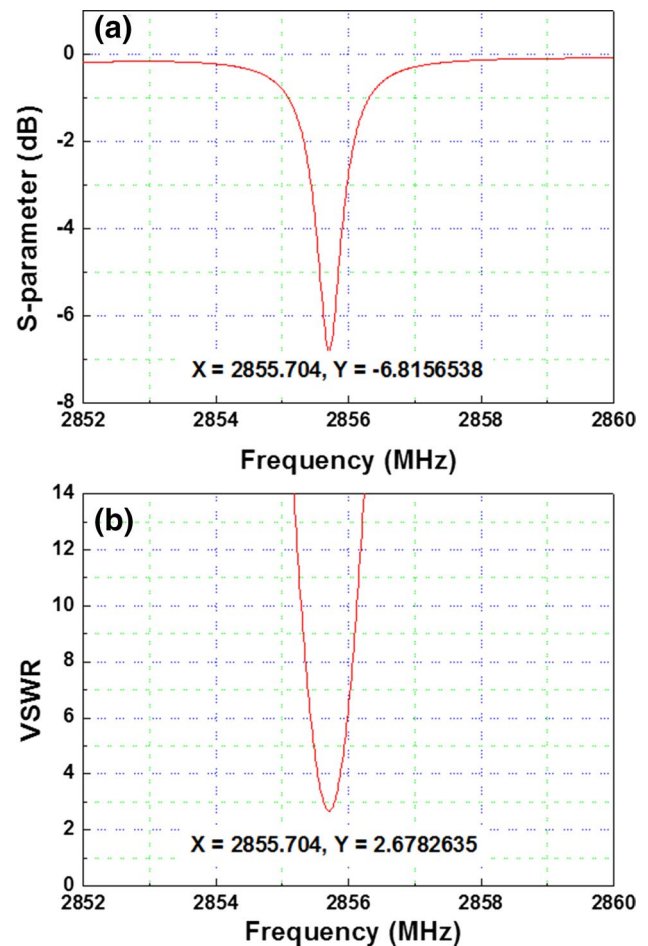

Fig. 8 S-parameter simulation results of the designed dual-energy electron accelerator cavity. **a** S-parameter and **b** VSWR results as a function of the frequency

from the electron gun calculated using the ASTRA code. Table 5 shows the initial beam parameters for the ASTRA simulation.

The average energy of the accelerated electron beam was confirmed to be 6.003 MeV and 2.993 MeV when the maximum electric field on the z-axis of the RF cavity was set to

Table 4 The final simulation results of the dual-energy electron accelerator cavity

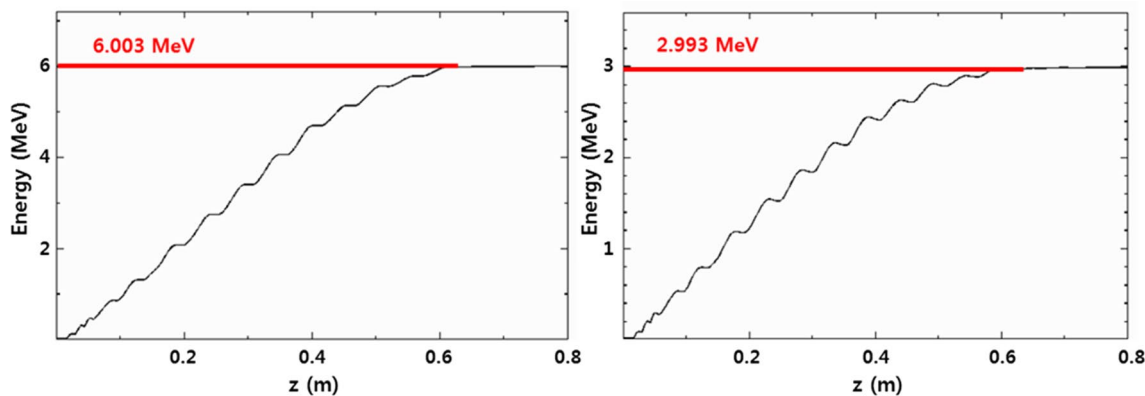| Simulation results of the designed cavity (S-band, $\pi/2$ mode)	
Frequency (MHz)	2855.7
Q-factor (unloaded)	15,976
Effective shunt impedance (MΩ/m)	87
Coupling coefficient	2.68
Total length (m)	0.57
E-field gradient (MV/m)	13.5
Number of cells	21

Fig. 9 The accelerated electron beam energy at an X-ray target position 80 cm away from the electron gun calculated using the ASTRA code

Table 5 Initial beam parameters for ASTRA simulation

Parameters	Value
Number of particles	200,000
Initial charge (nC)	0.2
Initial kinetic energy (keV)	20
Pulse width (ns)	1.05
RMS beam size (mm)	0.5

28.6 MV/m and 19.4 MV/m, respectively. This satisfies the design value of the dual-energy electron accelerator cavity. Figure 10 shows the transverse and longitudinal distributions of the 6 MeV accelerated electron beam at the target position. In Fig. 10a, the root-mean-square (RMS) size of the electron beam is 1.62 and 1.61 mm in the x- and y-axes, respectively. Figure 10b shows a longitudinal distribution of the electron beam until the bunching electron beam reaches n 80 cm distance from the electron gun. In Fig. 10b, the
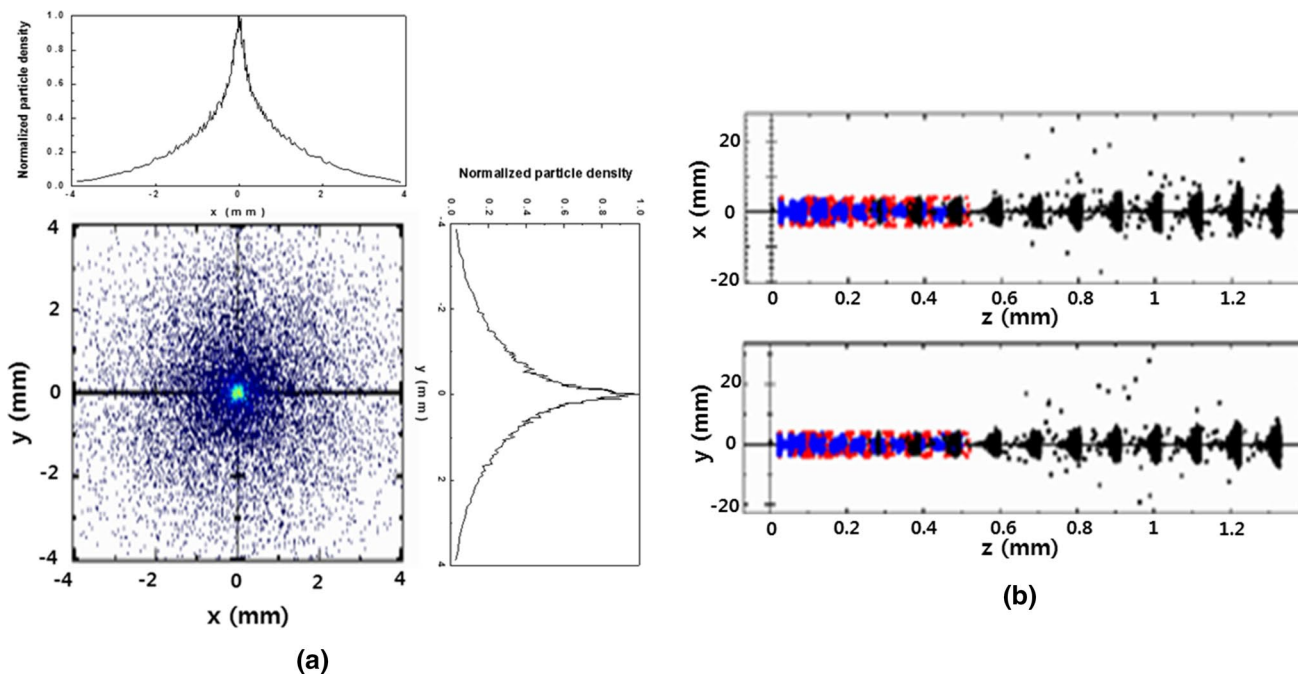

Fig. 10 The transverse (**a**) and longitudinal distributions (**b**) of the 6 MeV accelerated electron beam

Table 6 The results of the electron beam dynamics simulation of the dual-energy electron accelerator cavity

Parameters	6 MeV	3 MeV
Particles at the ends	87,618 (of 200,000)	80,549 (of 200,000)
Capture coefficient	43.8%	40.3%
Beam-size in x (σx)	1.62 mm (RMS)	1.43 mm (RMS)
Beam-size in y (σy)	1.61 mm (RMs)	1.43 mm (RMS)
Average electron energy	6.003 MeV	2.993 MeV
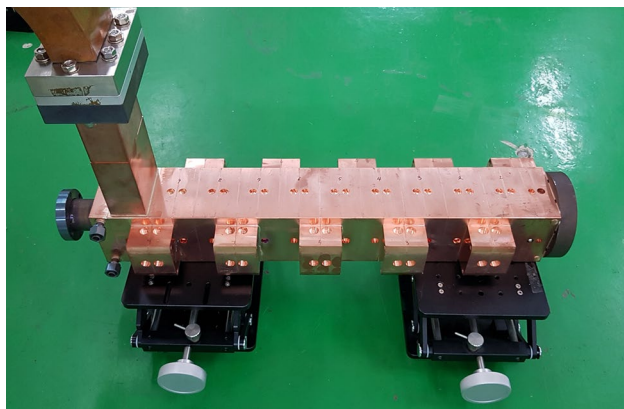
Fig. 11 The fabricated 6/3 MeV dual-energy electron accelerator cavity

upper and lower parts show the size of the electron beam in the x-axis and the y-axis, respectively. We found the electron beam proceeds well in forming a bunch along the period of the RF pulse. Table 6 shows the results of the electron beam dynamics simulation of the final designed dual-energy

accelerating cavity. In the optimized accelerating cavity, the average capture coefficient of the electron beam was 42.1%, and the beam size was found to be less than 2 mm (RMS). In addition, the calculated emittance was about 11 μm.

3 Experimental results

1. RF properties of the manufactured cavity

Figure 11 shows the fabricated 6/3 MeV dual-energy electron accelerator cavity using the final design parameters. The resonance frequency and coupling coefficient of the fabricated RF cavity can be obtained by measuring the S-parameter and VSWR of the RF cavity using a network analyzer (Agilent, model E5071C).

Figure 12 shows the results of the S-parameter (S11) measurements of the fabricated accelerating cavity using a network analyzer. The measured resonance frequency of the RF cavity is 2855.34 MHz, which is approximately 0.36 MHz different from the simulated result (2855.7 MHz). Since the resonance frequency range of the magnetron (e2V, model MG6028), which is an RF source to be used, is 2852–2861 MHz, the manufactured RF cavity is expected to operate stably in the operating range of the magnetron.

Figure 13 shows the measured results of the coupling coefficient at the power coupler. The VSWR shows the coupling coefficient is about 2.54 at a resonant frequency of 2855.34 MHz. The difference between the measured results and the simulated results (2.67) is about 0.13. The simulated and measured reflection losses of the incident RF power based on the coupling coefficient are about 0.2% and 0.3%, respectively. The reflection loss increased about 0.1% in the
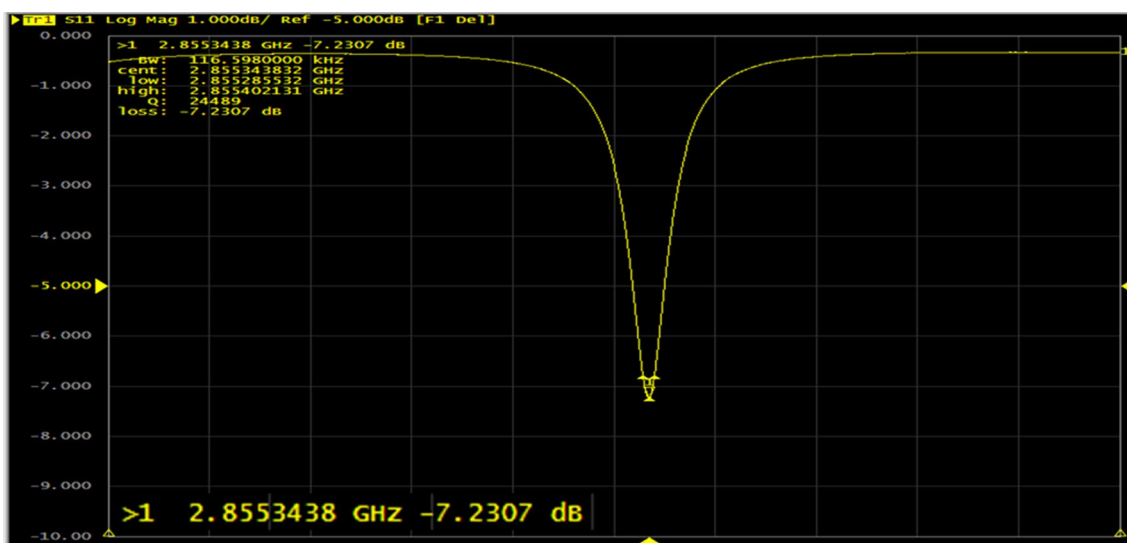
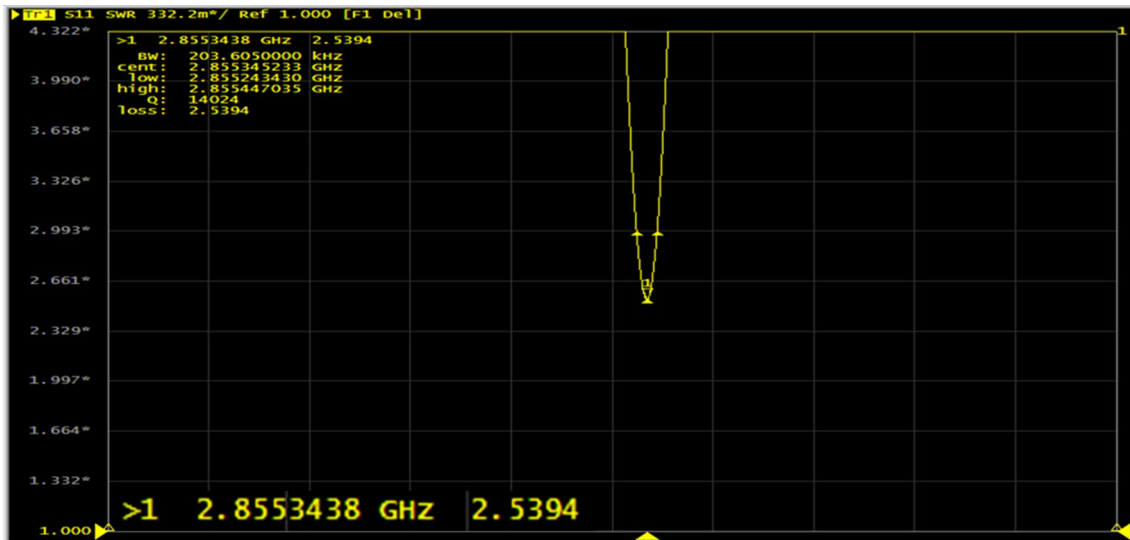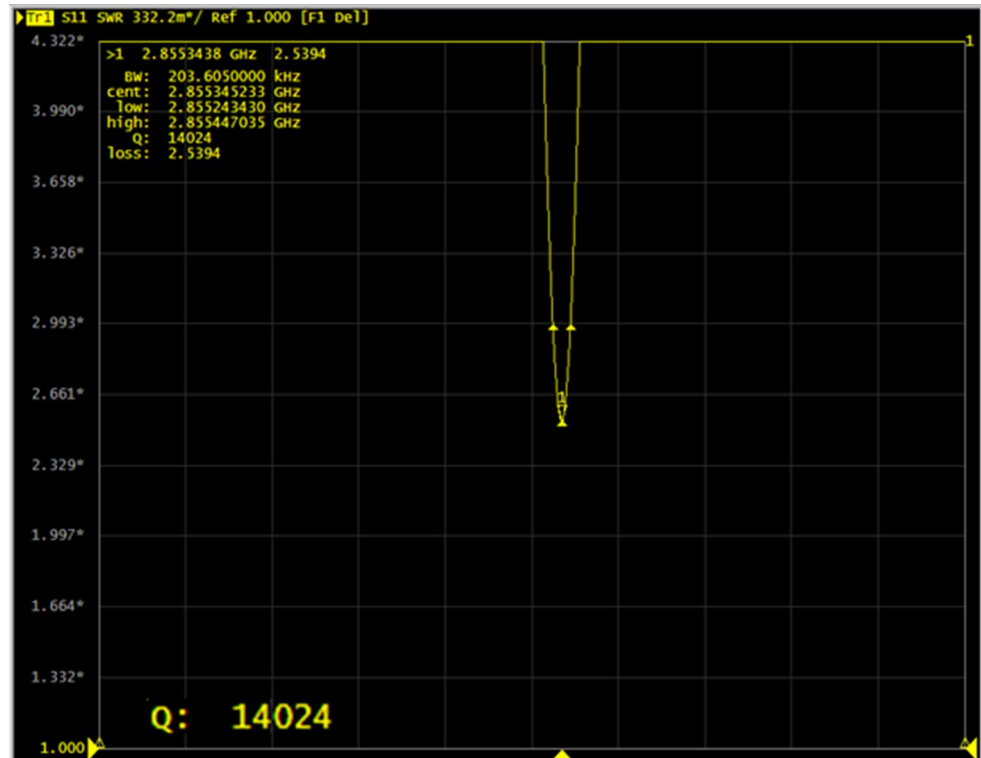**Fig. 12** The measured results of the S-parameter (S11) of the accelerator cavity

Fig. 13 The measurement results of the coupling coefficient at the power coupler

Fig. 14 The measurement results of the Q value of the RF cavity

manufactured cavity. This is caused by the differences in the resonant frequencies between the designed and manufactured cavities. Figure 14 shows the measurement results of the Q value of the manufactured RF cavity. The Q value of the manufactured RF cavity is 14024, which shows a difference of 1952 from the results of the simulation (15,976). The Q value is a parameter indicating the efficiency of the RF cavity. The higher the Q value, the higher the acceleration

efficiency of the RF cavity. The Q value was measured to be slightly lower because the reflection loss increased more than the simulation results in the coupling coefficient measurement.

A bead-pull test was performed to measure the electric field distribution inside the RF cavity. Figure 15 shows the setup for the bead-pull test. A small circular bead is fixed at a point on the insulating wire passing through the central

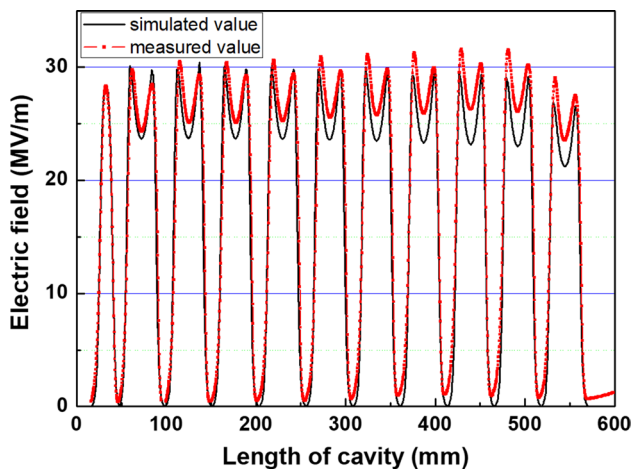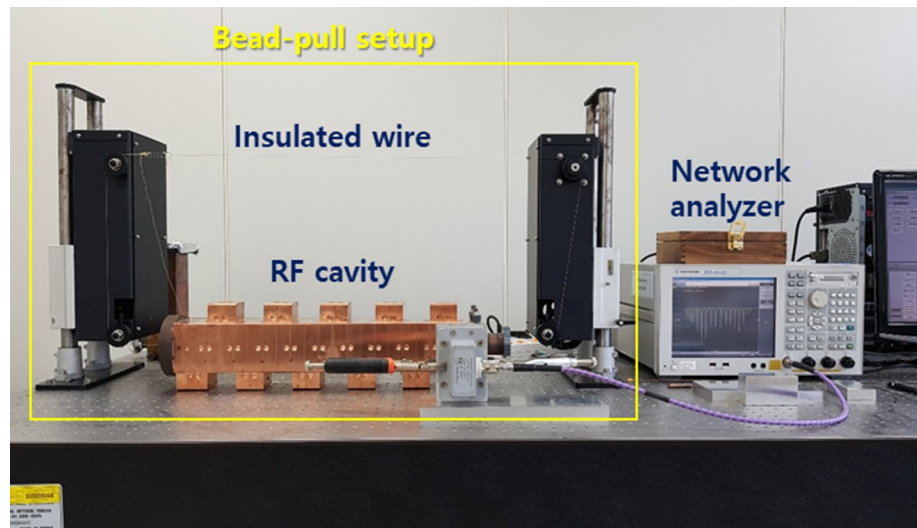**Fig. 15** The setup for a bead-pull test

Fig. 16 The measured results of the electric field distribution in the RF cavity by the bead-pull test. The black solid line represents the simulated results, and the red dotted line represents the measured results of the electric field distribution

axis of the RF cavity. The electric field distribution in the RF cavity is determined by measuring the change in the resonance frequency while the bead moves through the central axis of the RF cavity.

Figure 16 shows the measured results of the electric field distribution in the RF cavity by the bead-pull test. The black solid line represents the simulated results, and the red dotted line represents the measured results of the electric field distribution in the RF cavity. In the results, we infer the measured and simulated electric field distributions in the RF cavity are almost same. The uniformity of measured peak fields was calculated to be about 3%.

4 Conclusion

In this paper, we demonstrated the design and fabrication of the 6/3 MeV dual-energy RF accelerating cavity. Computational simulation of the RF cavity was carried out using 2-D and 3-D electromagnetic field analysis codes, and a real RF cavity was fabricated based on the simulation results. The manufactured RF cavity is a bi-periodic side-coupled $\pi/2$ mode type, and the resonant frequency is 2856 MHz. The designed RF cavity consists of a single bunching cell and 10 side-coupling cells and acceleration cells, respectively. In terms of the measured results, the resonance frequency is 2855.34 MHz, and the coupling coefficient and the Q value are 2.54 and 14,000, respectively. After completing the measurements, the accelerating tube will be tested for cooling and vacuum, and then the RF conditioning of the accelerating cavity will be carried out in combination with the RF devices. The fabricated 6/3 MeV dual-energy electron accelerating cavity is a side-coupled $\pi/2$ mode type and can be fabricated as a relatively small size compared to a conventional π-mode accelerating cavity. In addition, this RF cavity has a wide mode separation and can be operated stably. Therefore, it has great commercial advantages in terms of miniaturization and cost reduction. In addition, a dual-energy X-ray generated from the 6/3 MeV dual-energy electron accelerator can be used for the future security screening and nondestructive inspection markets because it not only can obtain a great transmission image, but also organic/inorganic substance information from the objects being inspected.

References

1. S. Hanna, *RF Linear Accelerators for Medical and Industrial Applications* (Artech House, 2012)
2. S. Ogorodnilov et al., Phys. Rev. ST Accel. Beams **5**, 104701 (2002)
3. A. V. Mishin, In: Proceedings of 2005 Particle Accelerator Conference, p. 240 (2005)
4. M. I. Ayzatsky et al., In: Proceedings of 2003 Particle Accelerator Conference, p. 2878 (2003)
5. W. W. Sapp et al., In: AIP Conference Proceedings **576**, p. 1057 (2001)
6. X.-W. Wang et al., High Energy Phys. Nucl. Phys. **31**(11), 1076 (2007)
7. A. Saverskiy et al., Phys. Proc. **66**, 232 (2015)
8. G. Chen et al., Nucl. Instrum. Methods Phys. Res. **B261**, 356 (2007)
9. S. Kutsaev et al., Phys. Proc. **90**, 115 (2017)
10. B.-N. Lee et al., J. Korean Phys. Soc. **64**, 205 (2014)
11. C.-X. Tang, Rev. Accel. Sci. Tech. **8**, 143 (2015)
12. C.–X. Tang et al., Int. Topical Meeting on Nuclear Research Applications and Utilization of Accelerators (IAEA, Vienna, Austria: 4–8 May 2009), p. 126
13. T. S. Dixit et al., In: PAC09 Conference Proceedings, p. 2021 (2009)
14. R. Krishnan et al., In: PAC09 Conference Proceedings, p. 4969 (2009)
15. H.B. Zhao et al., Nucl. Instrum. Methods Phys. Res. **A356**, 552 (1995)
16. K. Irie et al., Japan. J. Appl. Phys. **12**, 277 (1973)
17. Y. Kamino et al., Med. Phys. **34**, 1797 (2007)
18. T.P. Wangler, *Principles of RF Linear Accelerators* (Wiley-VCH, Weinheim, 2008)
19. J. Gao, Nucl. Instrum. Methods Phys. Res. **A309**, 5 (1991)
20. J. Gao, Nucl. Instrum. Methods Phys. Res. **A311**, 437 (1992)